GEOPHYSICS, VOL. 36, NO. 5 (OCTOBER 1971), P. 919-937, 13 FIGS., 1 TABLE

INVESTIGATION OF MAGNETIZATION AND DENSITY OF A NORTH ATLANTIC SEAMOUNT USING POISSON'S THEOREM†

LINDRITH CORDELL* AND PATRICK T. TAYLOR‡

The relationship between the gravitational and magnetic potentials caused by a uniform distribution of mass and magnetization may be used to obtain independent information about these physical properties. The general relationship in the frequency domain between the Fourier transforms of the gravity and magnetic anomaly fields is established through the Poisson theorem. The discrete Fourier transforms of the sampled continuous functions are used in an analysis which leads to a system of linear equations involving terms in density, magnetization, and calculated finite Fourier-series coefficients. A least squares solution of the system yields the three components of the total magnetization vector divided by the density. From these results, the direction of total magnetization and the minimum of the Koenigsberger ratio Q can be determined uniquely. The remanent magnetization direction and certain other information can be derived for special cases in which the value of one or more of the physical property terms can be assigned. Accurate results were obtained in the analysis of data from a theoretical model.

Analysis of gravity and magnetic data from the North Atlantic Gilliss seamount indicates the presence of a significant component of remanent magnetization and leads to derived physical properties which are in fairly close agreement with dredged sample data. The calculated direction of remanent magnetization indicates a paleomagnetic pole position in eastern Siberia, in general agreement with the predicted position for a Cretaceous source in the North Atlantic. The seamount example illustrates certain contingent problems to be considered in practical application of the method.

INTRODUCTION

The physical properties associated with local anomalies in the earth's gravitational and magnetic intensity fields are density, magnetic susceptibility, and remanent magnetization—in all, two scalars and the three components of a vector. Although in general each of these quantities is a point function in three-dimensional space within the disturbing body, for simplicity, we often consider the case of uniform physical properties. In this case, the field intensity at an exterior point can be represented by a physical property constant multiplying a volume integral. Most studies seek to solve the volume integral for the shape of the source in terms of measured field data and assumed physical properties. In paleomagnetic and certain other applications, the shape is assumed and the physical properties themselves are deduced. Either way, consideration of the physical properties is essential and we would like to exploit any information which is inherent in the data as a consequence of physical theory.

Bott et al (1966) have shown that, for the case of a finite source and uniform direction of magnetization, the range of the total magnetization direction can be deduced from magnetic intensity data by means of Poisson's theorem, without explicitly considering the volume integral. Where both magnetic intensity data and the shape of

† Publication authorized by the Director, U. S. Geological Survey. Manuscript received by the Editor February 1, 1971; revised manuscript received May 12, 1971.

* U. S. Geological Survey, Silver Spring, Maryland 20910.

‡ U. S. Naval Oceanographic Office, Washington, D. C. 20390.

the disturbing body are known, the integral can be evaluated directly, yielding a solution (in the sense of least squares) for the magnetic properties [see, e.g., Vacquier (1962), Henderson and Allingham (1964), Talwani (1965), Grossling (1967)]. Bhattacharyya (1967) has shown, by means of Fourier integral transforms, that it is theoretically possible to deduce the total magnetization vector from a knowledge of the gravity and magnetic intensity fields, even though the shape of the disturbing body is unknown; and R. G. Agarwal (1968), in an unpublished thesis, and Kanasewich and Agarwal (1970) effected the predicted deduction by using discrete Fourier series for the case of induced magnetization. In addition to the recent work cited above, many other topical geophysical studies have made use of Poisson's equation, especially after the publication of Garland's classic study in 1951. In this paper, we discuss a direct general method, also based on discrete Fourier series, for the combined analysis of gravity and magnetic data in terms of magnetization and density. We consider specifically the problems of identifying the remanent magnetization direction of a North Atlantic seamount and, from this identification, of determining the seamount's position with respect to the earth's inducing magnetic field at the time magnetization was acquired.

DERIVATIONS

In general, the gravitational potential U at an exterior point $\mathbf{p}$ due to an arbitrary continuous distribution of matter at body point $\mathbf{q}$ in three dimensions can be represented as

$$U(\mathbf{p}) = \gamma \int_{\text{volume}} \rho(\mathbf{q}) \frac{1}{|\mathbf{p}-\mathbf{q}|}\, dv, \quad (1)$$

and the magnetic potential V of a continuous distribution of magnetic material in the same system can be represented as

$$V(\mathbf{p}) = -\int_{\text{volume}} \mathbf{J}(\mathbf{q}) \cdot \nabla_p \left(\frac{1}{|\mathbf{p}-\mathbf{q}|}\right) dv, \quad (2)$$

where

$\rho(\mathbf{q})$ = density,

$\mathbf{J}(\mathbf{q})$ = magnetization, and

γ = gravitational constant.

If we consider the special case of uniform physical properties within the same closed volume,

$$U(\mathbf{p}) = \gamma\rho \int_{\text{volume}} \frac{1}{|\mathbf{p}-\mathbf{q}|}\, dv$$

and

$$\left(\frac{1}{\gamma\rho}\mathbf{J}\cdot\nabla\right) U(\mathbf{p}) = \int_{\text{volume}} \mathbf{J}\cdot\nabla \frac{1}{|\mathbf{p}-\mathbf{q}|}\, dv = -V(\mathbf{p}),$$

giving the well-known theorem (attributed to Poisson)

$$V = \frac{-1}{\gamma\rho} \nabla U \cdot \mathbf{J}. \quad (3)$$

For a body in a constant magnetic field $\mathbf{H}$, we represent the magnetization as

$$\mathbf{J} = J\mathbf{t}_0 = \kappa H \boldsymbol{\tau}_0 + J_N \mathbf{r}_0, \quad (4)$$

where

κ = magnetic susceptibility,

H = intensity of the (earth's) inducing field in the direction of the unit vector $\boldsymbol{\tau}_0$,

J_N = intensity of the natural remanent magnetization in the direction of the unit vector $\mathbf{r}_0$, and

J = intensity of total magnetization in the direction of the unit vector $\mathbf{t}_0$.

The direction cosines of the unit vectors

$\tau_{01} = \cos I \cos D,$
$\tau_{02} = \cos I \sin D,$
$\tau_{03} = \sin I,$
$r_{01} = \cos\theta \cos\sigma,$
$r_{02} = \cos\theta \sin\sigma,$ and
$r_{03} = \sin\theta$

are obtained from the induced and remanent azimuth angles D and σ measured clockwise from the positive x direction, and the induced and remanent inclination angles I and θ, measured as shown in Figure 1.

In the case of aeromagnetic surveys, the measured scalar quantity ΔT represents the relative magnitude of the magnetic field, which, provided that $\Delta T \ll H$, is given by

$$\Delta T = -\nabla V \cdot \boldsymbol{\tau}_0. \quad (6)$$

In the case of gravity surveys, the measured

scalar quantity Δg represents the relative magnitude of the gravitational field. Then, where Δg is small relative to the main earth's field,

$$U(x, y, z) = \int_{-\infty}^{z} \Delta g(x, y, \zeta) d\zeta, \qquad (7)$$

and, in view of equations (3) and (6),

$$\begin{aligned} \Delta T(x, y, z) &= \frac{1}{\gamma\rho} [\nabla(\nabla U \cdot \mathbf{J})] \cdot \boldsymbol{\tau}_0 \\ &= \frac{J}{\gamma\rho} \int_{-\infty}^{z} [\mathbf{t}_0 \cdot \nabla][\boldsymbol{\tau}_0 \cdot \nabla] \\ &\quad \cdot \Delta g(x, y, \zeta) d\zeta. \end{aligned} \qquad (8)$$

Noting that the gradient operator ∇ in the frequency domain has the form

$$\nabla \equiv 2\pi(i\hat{x}\mathbf{i}_0 + i\hat{y}\mathbf{j}_0 + \sqrt{\hat{x}^2 + \hat{y}^2}\mathbf{k}_0),$$

we take the Fourier transform of both sides of equation (8). Collecting terms leads to

$$\widehat{\Delta T}(\hat{x}, \hat{y}) = \left(\mathbf{C} \cdot \frac{J}{\rho} \mathbf{t}_0\right) \widehat{\Delta g}(\hat{x}, \hat{y}), \qquad (9)$$

where "$\widehat{\ }$" denotes the complex integral transform in the domain of the corresponding "frequency" variables $\hat{x}$ and $\hat{y}$, and

$$\begin{aligned} \mathbf{C} = \frac{2\pi}{\gamma} e^{2\pi\sqrt{\hat{x}^2+\hat{y}^2}z} \Bigg\{ &\left[\frac{-\hat{x}^2\tau_{01}}{\sqrt{\hat{x}^2+\hat{y}^2}} - \frac{\hat{x}\hat{y}\tau_{02}}{\sqrt{\hat{x}^2+\hat{y}^2}} + i\hat{x}\tau_{03} \right] \mathbf{i}_0 \\ &+ \left[\frac{-\hat{x}\hat{y}\tau_{01}}{\sqrt{\hat{x}^2+\hat{y}^2}} - \frac{\hat{y}^2\tau_{02}}{\sqrt{\hat{x}^2+\hat{y}^2}} + i\hat{y}\tau_{03} \right] \mathbf{j}_0 \\ &+ [i\hat{x}\tau_{01} + i\hat{y}\tau_{02} + \sqrt{\hat{x}^2+\hat{y}^2}\tau_{03}]\mathbf{k}_0 \Bigg\}. \end{aligned} \qquad (10)$$

Inasmuch as $\mathbf{C}$ involves only known terms of frequency, datum level, and direction cosines $\boldsymbol{\tau}_0$ of the earth's inducing field, equation (9) provides the linear system

$$\begin{aligned} C_1\left(\frac{J}{\rho} t_{01}\right) + C_2\left(\frac{J}{\rho} t_{02}\right) \\ + C_3\left(\frac{J}{\rho} t_{03}\right) = \frac{\widehat{\Delta T}(\hat{x}, \hat{y})}{\widehat{\Delta g}(\hat{x}, \hat{y})}, \end{aligned} \qquad (11)$$

which can be solved for the three unknowns $[(J/\rho)\mathbf{t}_0]$ in the sense of least squares.

In practice, the gravity and magnetic fields are of necessity represented as discrete samplings over a finite area, from which we obtain the corresponding discrete Fourier transforms by means of the fast Fourier transform computer algorithm (Cooley and Tukey, 1965). The discrete and integral Fourier transforms are fundamentally different (see, e.g., Gentleman and Sande, 1966). However, we can recast the results given in equation (11) in terms of the discrete transforms if we make a few more assumptions about the gravity and magnetic fields.

Further details of the analysis can at this point be deferred to the appendix. In summary, we digitize the magnetic and gravity data fields on an N_1 by N_2 array and we stipulate (by way of the requisite conditions) that the grid mesh is sufficiently fine and that the data fields tend smoothly to a constant value (normally zero) along the boundary. From the discrete data arrays, we obtain the discrete Fourier transforms

$$\begin{aligned} A^T_{k_1k_2} &= \frac{1}{N_1N_2} \sum_{j_1=0}^{N_1-1} \sum_{j_2=0}^{N_2-1} \Delta T_{j_1j_2} \\ &\quad \cdot e^{-2\pi i(j_1k_1/N_1 + j_2k_2/N_2)} \\ A^g_{k_1k_2} &= \frac{1}{N_1N_2} \sum_{j_1=0}^{N_1-1} \sum_{j_2=0}^{N_2-1} \Delta g_{j_1j_2} \\ &\quad \cdot e^{-2\pi i(j_1k_1/N_1 + j_2k_2/N_2)}; \end{aligned} \qquad (12)$$

$$\text{for } \begin{matrix} k_1 \\ k_2 \end{matrix} = 0, 1 \cdots \begin{matrix} N_1 - 1 \\ N_2 - 1 \end{matrix}$$

Substituting k_1/N_1 for $\hat{x}$, k_2/N_2 for $\hat{y}$, $A^T_{k_1k_2}$ for $\widehat{\Delta T}(\hat{x}, \hat{y})$, and $A^g_{k_1k_2}$ for $\widehat{\Delta g}(\hat{x}, \hat{y})$, we recast equations (10) and (11) in terms of the discrete transforms and carry out the least squares solution of equation (11) for $[(J/\rho)\,\mathbf{t}_0]$.

Noting that $\mathbf{t}_0$, $\mathbf{r}_0$, and $\boldsymbol{\tau}_0$ are unit vectors, we have

$$\frac{J}{\rho} = \left| \left(\frac{J}{\rho} \mathbf{t}_0\right) \right| \quad \text{and} \qquad (13)$$

$$\mathbf{t}_0 = \frac{1}{\left(\frac{J}{\rho}\right)} \left(\frac{J}{\rho} \mathbf{t}_0\right). \qquad (14)$$

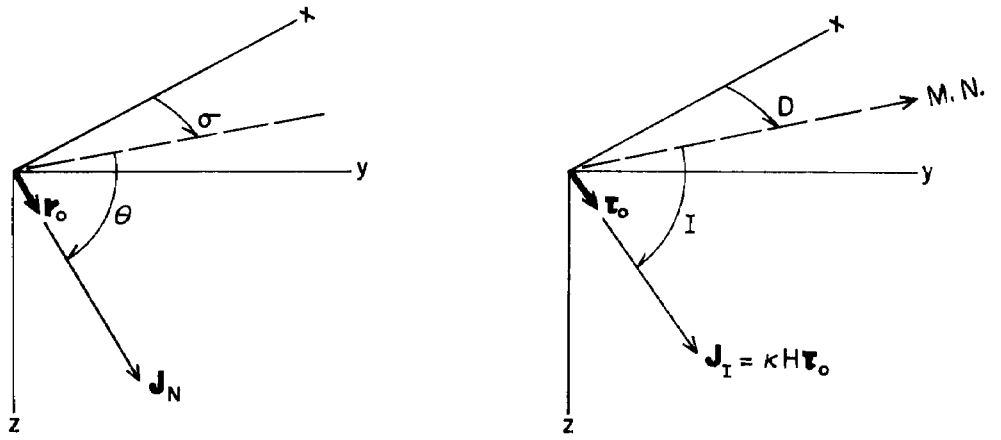

FIG. 1. Magnetization orientation diagram.

Obviously, the vectors $\kappa H\boldsymbol{\tau}_0$ and $J_N\mathbf{r}_0$ and their resultant $J\mathbf{t}_0$ are coplanar. As illustrated by the hypothetical situation shown in this plane of magnetic polarity in Figure 2, $\boldsymbol{\tau}_0$ and $\mathbf{t}_0$ are fixed, and $\mathbf{r}_0$ is free to sweep through the arc $\pi-\beta$, depending on the magnitude of the Koenigsberger ratio Q. The minimum possible value of Q obtains when $\mathbf{r}_0$ and $\mathbf{t}_0$ are perpendicular. Two directions of $\mathbf{r}_0$ are possible when $Q_{\min}<Q<1$. Thus, the minimum possible value of Q can be uniquely determined, and

$$Q_{\min}\Big| \begin{array}{l} = \sqrt{1-(\mathbf{t}_0\cdot\boldsymbol{\tau}_0)^2}; \quad (\mathbf{t}_0\cdot\boldsymbol{\tau}_0) > 0 \\ = 1; \quad \text{otherwise.} \end{array} \tag{15}$$

For $\beta<\pi/2$, the minimum possible value of J_N obtains when $\mathbf{r}_0$ and $\boldsymbol{\tau}_0$ are perpendicular, and, in general,

$$J_{N_{\min}}\Big| \begin{array}{l} = J\sqrt{1-(\mathbf{t}_0\cdot\boldsymbol{\tau}_0)^2}; \quad (\mathbf{t}_0\cdot\boldsymbol{\tau}_0) > 0 \\ = J; \quad \text{otherwise.} \end{array}$$

The ratio J/ρ can be evaluated by means of equa-

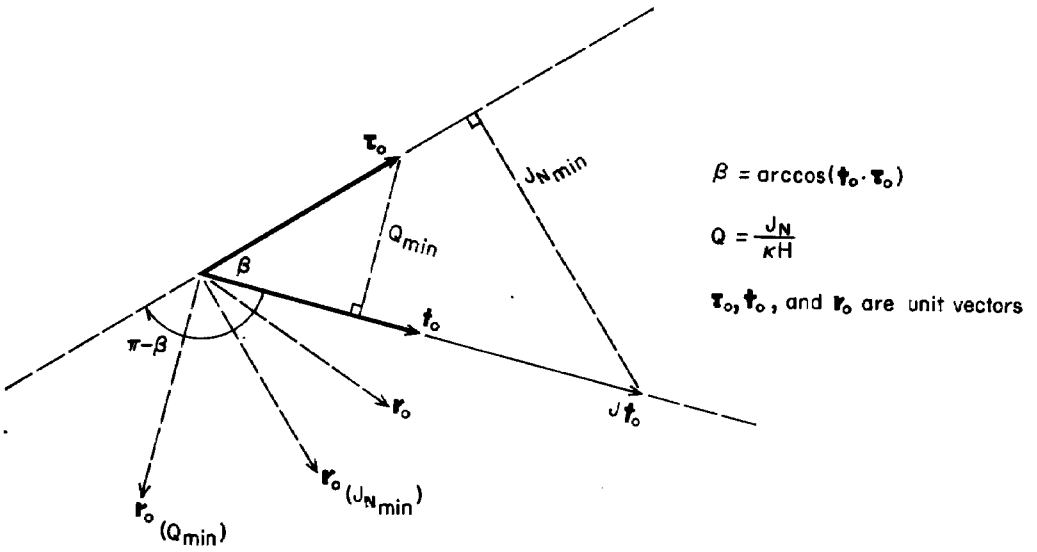

FIG. 2. Vector diagram in plane of magnetic polarization.

tion (13). Denoting this quantity by R, we obtain

$$J_{N_{\min}} \begin{cases} = \rho R\sqrt{1-(\mathbf{t}_0\cdot\boldsymbol{\tau}_0)^2}; & (\mathbf{t}_0\cdot\boldsymbol{\tau}_0) > 0 \\ = \rho R; & \text{otherwise, where} \end{cases} \tag{16}$$

$$R = \left(\frac{J}{\rho}\right) \text{ as evaluated in equation (13).}$$

Thus, although the minimum possible value of J_N cannot be determined uniquely, it can be stated as a function of density, which normally can be estimated within a narrow range.

Normalizing equation (4) with respect to J_N and combining terms, we find that

$$\mathbf{r}_0 \begin{cases} = \dfrac{1}{Q}\left[(\mathbf{t}_0\cdot\boldsymbol{\tau}_0 + \sqrt{(\mathbf{t}_0\cdot\boldsymbol{\tau}_0)^2 - 1 + Q^2})\mathbf{t}_0 - \boldsymbol{\tau}_0\right]; & Q \geq 1 \\ = \dfrac{1}{Q}\left[(\mathbf{t}_0\cdot\boldsymbol{\tau}_0 \pm \sqrt{(\mathbf{t}_0\cdot\boldsymbol{\tau}_0)^2 - 1 + Q^2})\mathbf{t}_0 - \boldsymbol{\tau}_0\right]; & Q < 1, \end{cases} \tag{17}$$

in which the remanent magnetization unit vector $\mathbf{r}_0$ is determined uniquely as a function of Q. Then, from equation (5),

$$\sigma = \text{azimuth of remanent magnetization} = \arctan\left(\frac{r_{0_2}}{r_{0_1}}\right) \tag{18}$$

and

$$\theta = \text{remanent inclination} = \arcsin(r_{0_3}).$$

Finally, we can combine several of the equations into the form

$$\rho(\kappa, Q) \begin{cases} = \dfrac{\kappa H}{R}\left[(\mathbf{t}_0\cdot\boldsymbol{\tau}_0) + \sqrt{(\mathbf{t}_0\cdot\boldsymbol{\tau}_0)^2 - 1 + Q^2}\right]; & Q \geq 1 \\ = \dfrac{\kappa H}{R}\left[(\mathbf{t}_0\cdot\boldsymbol{\tau}_0) \pm \sqrt{(\mathbf{t}_0\cdot\boldsymbol{\tau}_0)^2 - 1 + Q^2}\right]; & Q < 1 \end{cases} \tag{19}$$

and inasmuch as the quantities R [see equation 16] and $(\mathbf{t}_0\cdot\mathbf{r}_0)$ can be evaluated, we obtain a surface equation in terms of the essential scalar quantities κ, Q, and ρ.

DISCUSSION AND THEORETICAL EXAMPLE

As noted previously, the physical property terms and the space and body boundary terms differ in mathematical structure within the potential field equations. For the case of gravity and magnetic force fields related to a common and homogeneous source, we have sought to organize those physical property relationships which can be derived from the data without knowing the shape of the source. The ratio J/ρ [equation (13)], the total magnetization direction $\mathbf{t}_0$ [equation (14)], and the minimum possible value of the Koenigsberger ratio Q [equation (15)] can be determined uniquely. Use of the other relationships requires that certain parameters be assigned, the realization of which will depend on the circumstances. The minimum possible magnitude of remanent magnetization can be determined in terms of estimated density [equation (16)]. The direction of remanent magnetization, indicated by the unit vector $\mathbf{r}_0$, can be determined in terms of an assigned value or suite of values of Q [equation (17)]. The essential scalar quantities κ, Q, and ρ can be expressed independently of vector considerations in terms of the contour surface given in equation (19).

Obviously, the hypothesis of a common, uniform source is crucial. All geophysical modeling entails the concept of abstract, bulk physical properties representing physical quantities which are demonstrably variable. Here we require that homogeneity applies both to mass and magnetization throughout the same closed volume. Generally, homogeneity cannot be established independently and it definitely cannot be positively established a posteriori. That is to say, plausible results do not necessarily indicate that the sources are homogeneous, although the converse might be true in certain cases.

As an illustration and test of the numerical stability of the computations, we carry through the analysis on the vertical gravity and total magnetic intensity fields of a sphere. The anomalies were calculated on a 32 by 32 array having a grid interval of 2 km, with the following parameters:

D = inducing field declination = -20 degrees,
I = inducing field inclination = 65 degrees,
H = inducing field strength = 0.538 öersted,
κ = magnetic susceptibility = 0,
σ = remanent field declination = 20 degrees,
θ = remanent field inclination = 44 degrees,
J_N = strength of remanent magnetization = 2.44×10^{-3} emu/cm^3,
ρ = density = 1.0 gm/cm^3.

From these data, we obtained the values: $J/\rho = 2.43 \times 10^{-3}$ emu/gm (error = 0.49 percent), $\sigma = 20.31$ degrees (error = 1.55 percent), $\theta = 44.59$ degrees (error = 1.34 percent), and $Q_{\min} = 0.5$. For an identical model magnetized in the inducing field direction, we obtained, within an error of 1.4 percent, $\sigma = D$, $\theta = I$, and, in this case, $Q_{\min} = 0.0$. These solutions were based on the use of wavenumber terms up through 7. Tests with other reasonable wavenumber cutoffs and other synthetic data sets have all given results within a few percent of their actual values.

The ratio J/ρ and the unit vector $\mathbf{t}_0$, together with the magnetic anomaly ΔT, comprise the essential ingredients of the pseudogravity transformation (Baranov, 1967; and Bhattacharyya, 1967). Inasmuch as the physical property analysis takes place in the frequency domain, a comparison of the actual gravity anomaly with the pseudogravity anomaly based on the derived physical properties permits the derived results to be judged in the more familiar space domain.

Following the notation of equations (9) and (10), we can, to a close approximation, write the discrete Fourier-series coefficients $A^{g'}$ of the pseudogravity anomaly as

$$A^{g'}_{k_1 k_2} = \frac{1}{\frac{J}{\rho}\,(\mathbf{C}\cdot\mathbf{t}_0)}\, A^{T}_{k_1 k_2},$$

recognizing that the $A^{g'}_{0,0}$ term is undefined and that certain spectral symmetries must be used to insure that the pseudogravity is real-valued. Then, supplying the derived values J/ρ, t_{0_1}, t_{0_2}, and t_{0_3}, we obtain the pseudogravity anomaly by the inverse transform

$$g'_{j_1 j_2} = \sum_{k_1=0}^{N_1-1} \sum_{k_2=0}^{N_2-1} A^{g'}_{k_1 k_2} \cdot e^{2\pi i \left(\frac{k_1 j_1}{N_1} + \frac{k_2 j_2}{N_2}\right)}. \qquad (20)$$

The gravity and pseudogravity based on the derived parameters are shown for the sphere model in Figure 3. In Figure 4, we compare the spectra of magnetic, gravity, and pseudogravity fields of the sphere model. The amplitude spectrum of the Fourier integral transform of the gravity anomaly of a sphere on a logarithmic scale is a straight line, with the $A_{0,0}$ intercept proportional to the total mass as a consequence of Gauss's theorem. In the case of the discrete transform, as shown in Figure 4, the high wavenumber terms are influenced by aliasing, and the $A_{0,0}$ term is low because the graphical integration is carried out only over a finite area. Except for these effects, the gravity and pseudogravity spectra for the idealized sphere model are virtually identical.

Assuming that the data grid interval s is sufficiently small that graphical integration may be accomplished by summation, we can express the anomalous Gauss mass M in terms of the inequality

$$M > \frac{N_1 N_2 s^2}{2\pi\gamma} A_{0,0}, \qquad (21)$$

understanding that expression (21) tends toward equality as the data grid becomes extensive relative to the anomaly, as it is in the case of the sphere example, although the assumption generally is not valid in the practical case. The actual mass of the sphere is 33.51×10^{15} gm, and the calculated $A^g_{0,0} = 0.312532$ mgal, giving a calculated mass of 30.18×10^{15} gm (error = 9.9 percent).

In practice, the gravity anomaly is not normally measured or identifiable far from the source, and the anomalous mass calculated in the way we have discussed will be considerably lower than the true mass (LaFehr, 1965). For the case of a compact source which can be approximated by a sphere, an alternative method is to fit a straight line to the lower few wavenumber points of the log spectral plot, and project the line back to determine the $k = 0$ intercept. For the sphere model (see Figure 4) $A^{\text{proj}}_{0,0} = 0.339$, giving a calculated mass of 32.73×10^{15} gm (error = 2.3 percent).

GEOPHYSICAL SURVEY OF GILLISS SEAMOUNT

From October 25 to 27, 1968, the USNS *SGT Shoup* conducted a detailed bathymetric, magnetic, and gravimetric study of the Gilliss seamount. The Gilliss seamount is located northeast

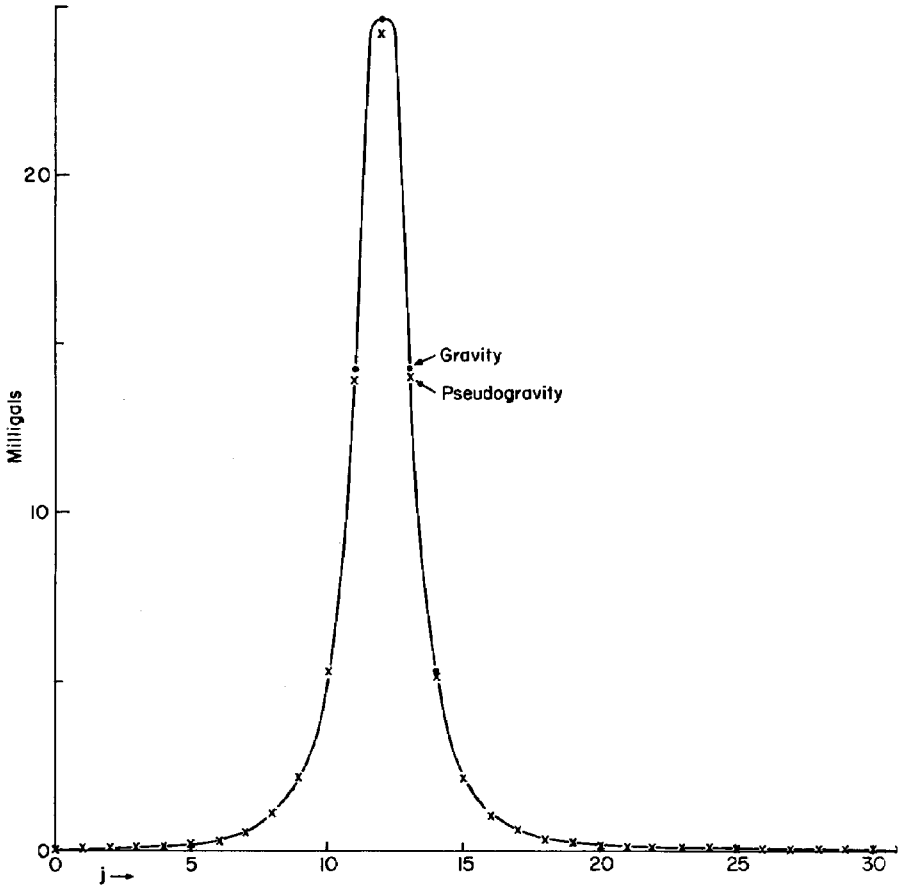

FIG. 3. Gravity and derived pseudogravity anomalies for sphere model.

of Bermuda at approximately 58°38′ W longitude and 35°35′ N latitude (Figure 5). This detailed survey was carried out to support other geological and geophysical studies of the seamount.

Navigational control was obtained from both satellite and Loran C. The ship's tracks from which data were obtained are shown in Figure 5.

There are approximately 365 line km of data from tracks primarily oriented east-west, and 187 line km of data from north-south and diagonally oriented tracks. The latter were obtained mainly for use as cross-checks in accuracy determinations. Distance between the east-west oriented tracks varied from about 5.5 km to 7.1 km.

A 12 khz precision graphic recorder (PGR) was used to record the bathymetric data. A corrected contour chart of these data is given in Figure 5. The contour interval is 100 fathoms.

Magnetic data were obtained by means of a Varian proton-precession magnetometer. No corrections were made for temporal variations, since the k indices for the period of this study were less than 3 (records obtained from the National Oceanic and Atmospheric Administration magnetic observatory at Fredricksburg, Virginia). Figure 6 shows the residual magnetic field of the Gilliss seamount obtained by removing the IGRF (Fabiano and Peddie, 1969) from the total intensity data and adjusting the resulting anomaly by+100 gammas. The contour interval is 50 gammas. The twin peaks of the Gilliss seamount (Figure 5) are indicated by the two small crosses on Figure 6. The magnetic highs are displaced to the southeast of the bathymetric highs. Hachured contours represent regions of negative magnetic field.

A Bell stable-table gravity meter was used to

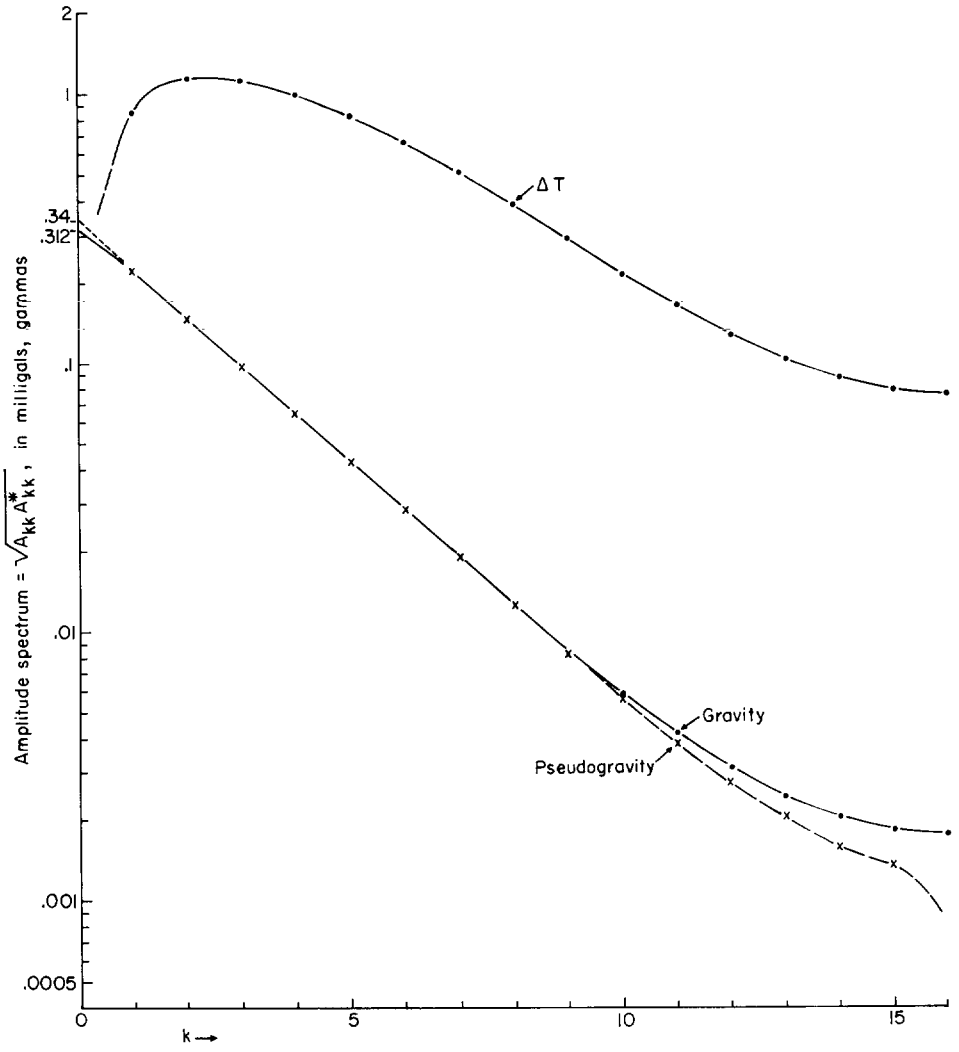

FIG. 4. Discrete amplitude spectra of ΔT, gravity, and pseudogravity fields of sphere model. Amplitude scale is logarithmic with decimal divisions.

gather the gravity data. Discrete data points represent weighted averages taken at 5 minute (1.5 km) intervals. From cross-checks, these data were considered to be accurate to +3 mgal. Navigational information was used to compute the free-air gravity anomaly, shown in Figure 7. The contour interval is 10 mgal. The value of the meandering contour is −30 mgal, which probably represents the regional gravity field in this area. Talwani and LePichon (1969) have shown that this region is in a geoidal depression within the western North Atlantic. Relative to the meandering contour, the amplitude of the anomaly is +70 mgal.

ANALYSIS OF GILLISS SEAMOUNT

Gravity and magnetic data over the Gilliss seamount were digitized on a 32 by 32 point grid having a grid interval of 1.5625 km. The area covered by the grid is indicated by corner tics in Figures 6 and 7. Solutions for a wavenumber cutoff of 1, 2, 3, 7, and 16 were obtained. Each of these solutions indicated virtually the same direction of total magnetization; however, the de-

rived value of J/ρ decreased systematically with increase in wavenumber cutoff, ranging from 4.67×10^{-3} to 2.44×10^{-3} emu/gm. Based on a wavenumber cutoff of 2 and the input parameters,

D = inducing field declination = -20.0 degrees,
I = inducing field inclination = 65.0 degrees,

and

H = inducing field strength = 53800 gammas,

we obtained

$$J/\rho = 3.29 \times 10^{-3} \text{ emu/gm},$$
$$t_{0_1} = -0.2704$$
$$t_{0_2} = -0.6753$$
$$t_{0_3} = 0.6862$$
$$Q_{\min} = 0.370$$

and

$$\beta(\mathbf{t}_0, \boldsymbol{\tau}_0) = 21.7 \text{ degrees.}$$

Amplitude spectra for the magnetic, gravity, and derived pseudogravity fields of Gilliss seamount are shown in Figure 8. Here the situation is less straightforward than with the sphere example shown in Figure 4. The greater attenuation of amplitude with wavenumber of the magnetic and related pseudogravity spectra, relative to

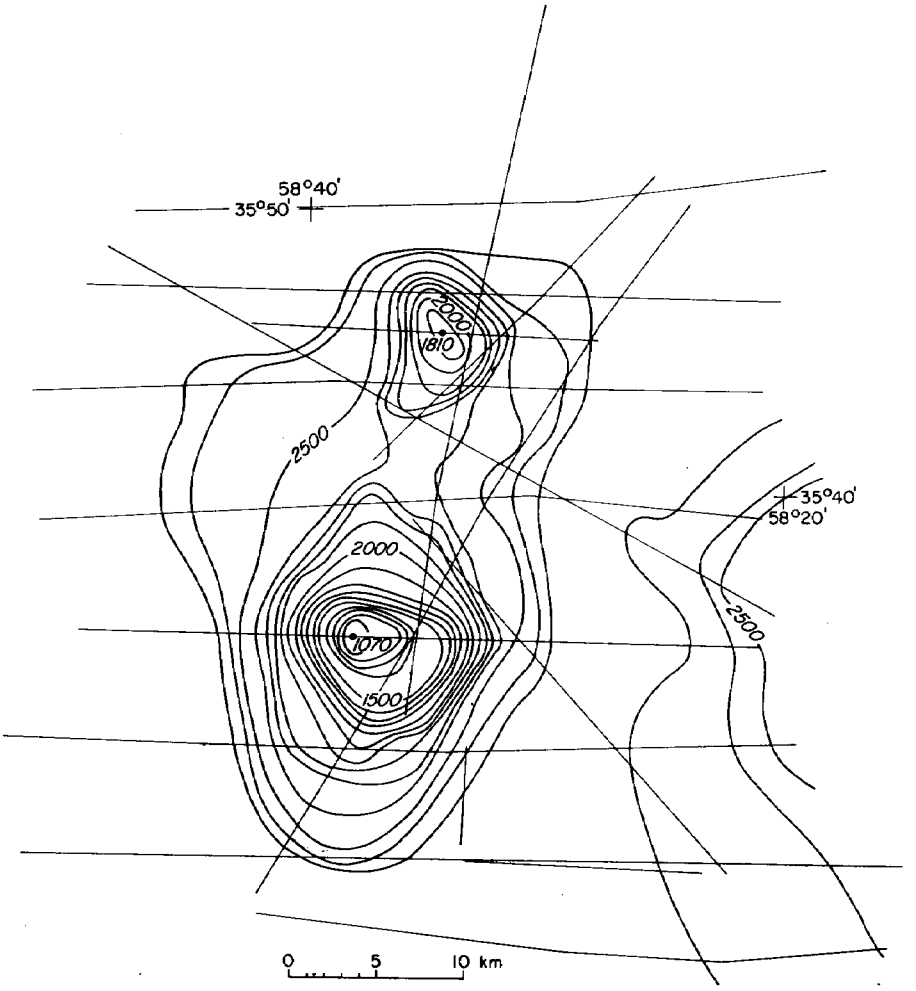

FIG. 5. Bathymetric map of Gilliss seamount showing ship's tracks. Contour interval is 100 fathoms.

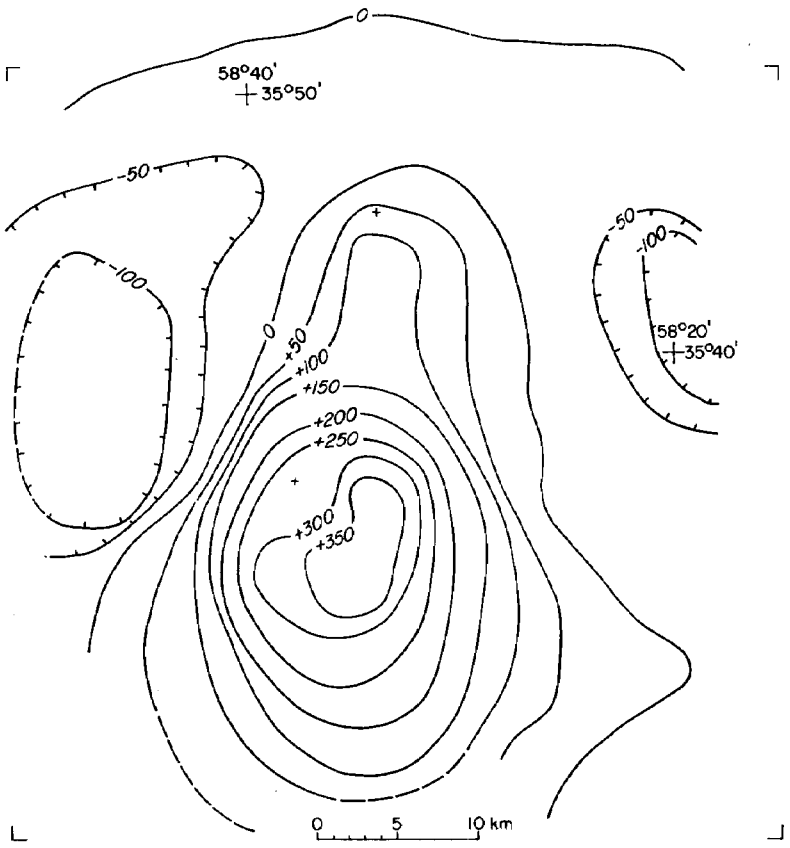

FIG. 6. Residual total-magnetic intensity map of Gilliss seamount. Contour interval is 50 gammas.

that of the actual gravity field, probably indicates that the magnetic source is deeper than the gravity source or that the J/ρ ratio increases with depth. These possibilities could be attributed either to the presence of a buried root (having a lower density contrast) or to the presence of a nonmagnetic outer mantle.

Using the lowest three-wavenumber terms, we obtain from the gravity spectrum the value $A_{0,0}^{\text{proj}} = 10.93$ [see Figure 8 and discussion of expression (21)], giving a Gauss mass of 652×10^{15} gm. The volume of the seamount above the base of 2700 fathoms (see Figure 5) is about 415×10^{15} cm^3. These figures together indicate a density contrast of 1.57 gm/cm^3, or an actual density of about 2.6 gm/cm^3. Inasmuch as this is a reasonable or even low value for the expected density of the seamount, we infer that if a buried root is present, its contribution to the gravity field is small. The same inference can be drawn from gravity modeling studies that use the system of Cordell and Henderson (1968); results of the model studies are not shown here.

There is, on the other hand, some basis for supposing that the outer mantle of the seamount is relatively nonmagnetic. This could be attributed to the scrambling of magnetic polarization due to structural movement or autobrecciation. It could also be attributed to decrease in magnetic intensity due to mixture with sedimentary rock. A total of 300 line km of seismic reflection profiles in the vicinity of the Gilliss seamount (Taylor and Hekinian, 1971) indicate that sediments, up to one km in thickness locally, cover parts of the seamount.

The gravity and pseudogravity fields based on the derived physical properties for the seamount data are shown in Figures 9 and 10. In general, the amplitude of a pseudogravity anomaly is inversely proportional to the ratio J/ρ, whereas its

position and trend are dependent on the assigned magnetization direction $\mathbf{t}_0$. As shown in the figures, the correspondence in position and trend between the pseudogravity and actual gravity fields is good, indicating that the derived total magnetization direction may be valid.

The amplitude of the pseudogravity anomaly presents a complicated problem. The pseudogravity analysis in both space and frequency domains seems to indicate that the magnetic source is deeper than the gravity source, and, although the arguments are tenuous, we suggest that this may be attributed to the presence of a weakly magnetic outer mantle. Given this hypothetical model, it would be desirable to separate from the gravity anomaly the component related to the presumably uniformly magnetic core, to which the analysis based on Poisson's relationship could be more validly applied. Although we have no basis for making this separation of gravity components, we can estimate the effect by constraining the pseudogravity anomaly within an envelope delimited by the actual gravity field. Thus, for this two-component model, we might reduce the pseudogravity profile shown in Figure 10 by a scale factor possibly as small as about 0.5. This scaling amounts to a corresponding increase in the factor J/ρ, and in view of the contingency discussed above, we should perhaps consider the value of J/ρ to be somewhere be-

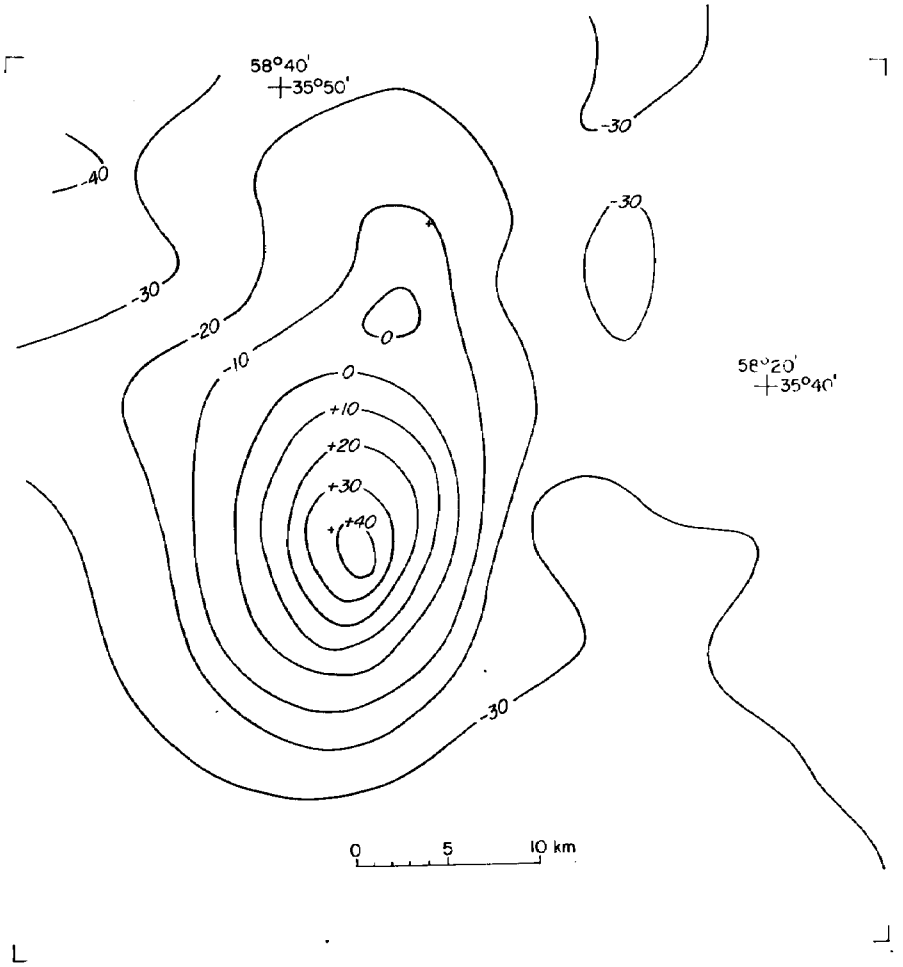

FIG. 7. Free-air gravity anomaly map of Gilliss seamount. Contour interval is 10 mgal.

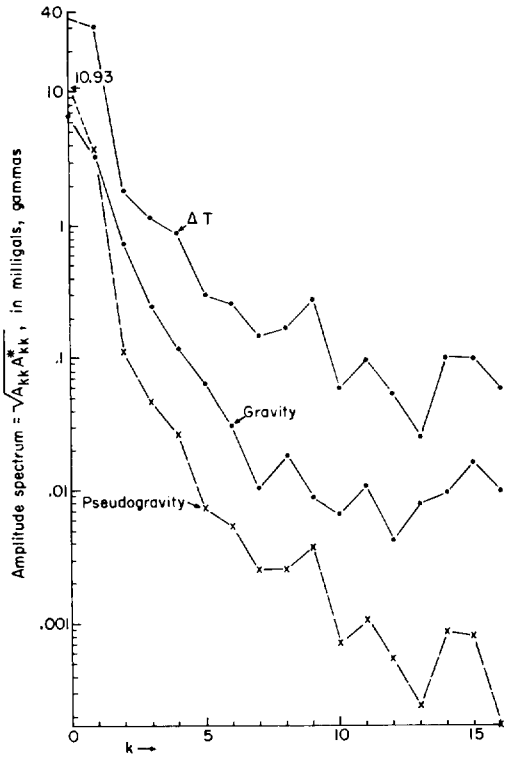

FIG. 8. Discrete amplitude spectra of ΔT, gravity, and pseudogravity fields of Gilliss seamount. Amplitude scale is logarithmic with decimal divisions.

tween the derived value of 3.29×10^{-3} and the value of 6.57×10^{-3} obtained by scaling down the pseudogravity profile—say

$$J/\rho = 4.93 \times 10^{-3} \pm 1.64 \times 10^{-3} \text{ emu/gm}.$$

Magnetic analyses of three basaltic samples obtained from dredging the Gilliss seamount are given in Table 1 (F. J. Vine, personal communication, 1970). Estimating the minimum density contrast to be about 1.5 gm/cm³, we find, from equation (16), that

$$J_{N_{\min}} = 2.19\times10^{-3} \pm 0.73\times10^{-3} \text{ emu/cm}^3;$$

thus, the derived values for $J_{N_{\min}}$ and $Q_{\min}$ appear to be in fairly close agreement with the sample data.

In Figure 11, we evaluate equation (19) for the derived Gilliss results over a range of κ between 0.1×10^{-3} and 10×10^{-3}, and over a range of Q

Table 1. Analyses of Gilliss dredge samples (F. J. Vine, Dept. of Environmental Sciences, Univ. of East Anglia, Norwich, England, Personal communication, 1970)

Sample	κ	J_N	Q
1	3.56×10^{-3}	10.67×10^{-3}	5.57
2	3.65×10^{-3}	1.136×10^{-3}	0.58
3	2.57×10^{-3}	2.438×10^{-3}	1.76

between $Q_{\min}=0.371$ and 100. The resulting surface, for $\rho(\kappa, Q)$, having a value between 0.5 and 3.0 gm/cm³, is contoured at an interval of 0.5 gm/cm³. Density in this case refers to density contrast with respect to sea water. Density contrast of the Gilliss seamount is probably within the range of 1.5 to 2.0 gm/cm³, so the ratio of κ to Q can be restricted within a rather narrow band, as can be seen on the figure. The sample values of κ and Q are indicated on their respective axes. Of the sampled parameters, susceptibility appears to be the more compactly clustered; and the mean of the measured susceptibility, together with the probable density range, indicate that Q has a value of about 3.

In paleomagnetic application, it is the vector $\mathbf{r}_0$, rather than the total magnetization vector $\mathbf{t}_0$, which must be considered. As shown in equation (17), this requires either that Q is known or that Q is known to be large. The latter situation is better, because Q cannot normally be accurately determined and because the direction of $\mathbf{r}_0$ is sensitive to small variation in Q where Q is small [cf. equation (17) and Figure 2]. In this regard, the results from the Gilliss data shown in Figure 11, if taken at face value, indicate that Q is probably sufficiently large to warrant proceeding with the determination of the remanent magnetization direction $\mathbf{r}_0$ by means of equation (17).

According to Doell and Cox (1961), the latitude ϕ', and longitude λ' of the virtual paleomagnetic pole in terms of the latitude ϕ, longitude λ, and remanent magnetization declination σ and inclination θ of the source are given by

$$\phi' = \arcsin(\sin\phi\cos p + \cos\phi\sin p\cos\sigma)$$

and

$$\lambda' \begin{cases} = \lambda + B; & \cos p \geq \sin\phi\sin\phi' \\ = \lambda + 180 - B; & \cos p < \sin\phi\sin\phi', \end{cases} \tag{22}$$

where

$$p = \arctan(2 \cot \theta)$$

and

$$B = \arcsin\left(\frac{\sin p \sin \sigma}{\cos \phi'}\right).$$

Latitudes ϕ and ϕ' are between 0 and 90 degrees, positive if north, negative if south; longitudes λ and λ' are between 0 and 180 degrees, positive if east, negative if west; declination $0 \leq \sigma \leq 360$ degrees is measured clockwise from true north; and inclination $0 \leq \theta \leq 90$ degrees is measured positive downward.

Evaluating equations (17) and (18) using the parameters derived from the analysis of the Gilliss data and a suite of Q between Q_{min} and infinity, we obtain the trace of the virtual paleomagnetic pole position as a function of Q shown in Figure 12. Pole positions corresponding to a Q of 0.6, 0.8, 1, 2, 3, 5, 10, and infinity are labeled. For $Q=3$, $\phi'=65°10'$ N, and $\lambda'=178°48'$. For $Q>2$, the position of the paleo-pole is restricted within a range of 5 degrees of latitude and 14 degrees of longitude, so if the actual value of Q for the seamount is close to the estimated value of 3 and if the derived total-magnetization direction is reasonably correct, the paleo-pole is located within fairly narrow limits. Foraminifers *Rugoglobigerina*

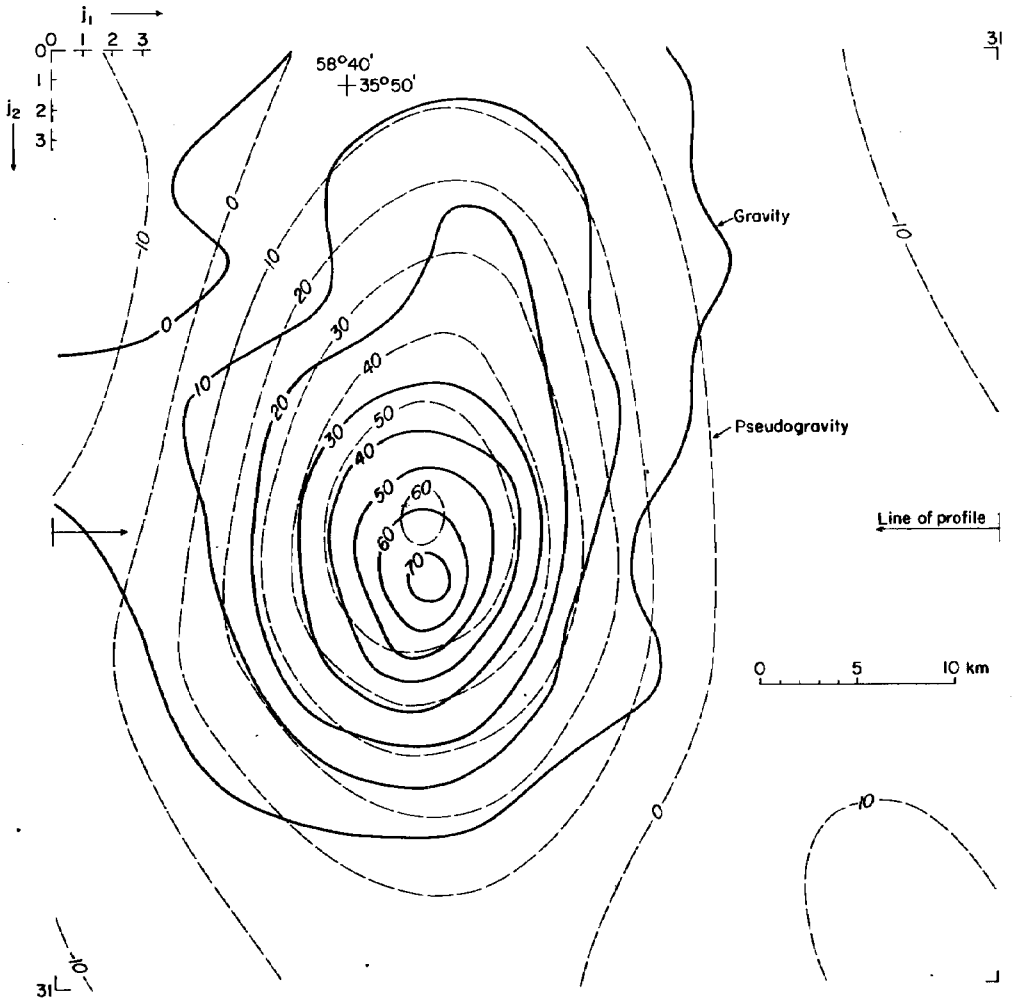

FIG. 9. Gravity and pseudogravity anomalies of Gilliss seamount. Contour interval is 10 mgal.

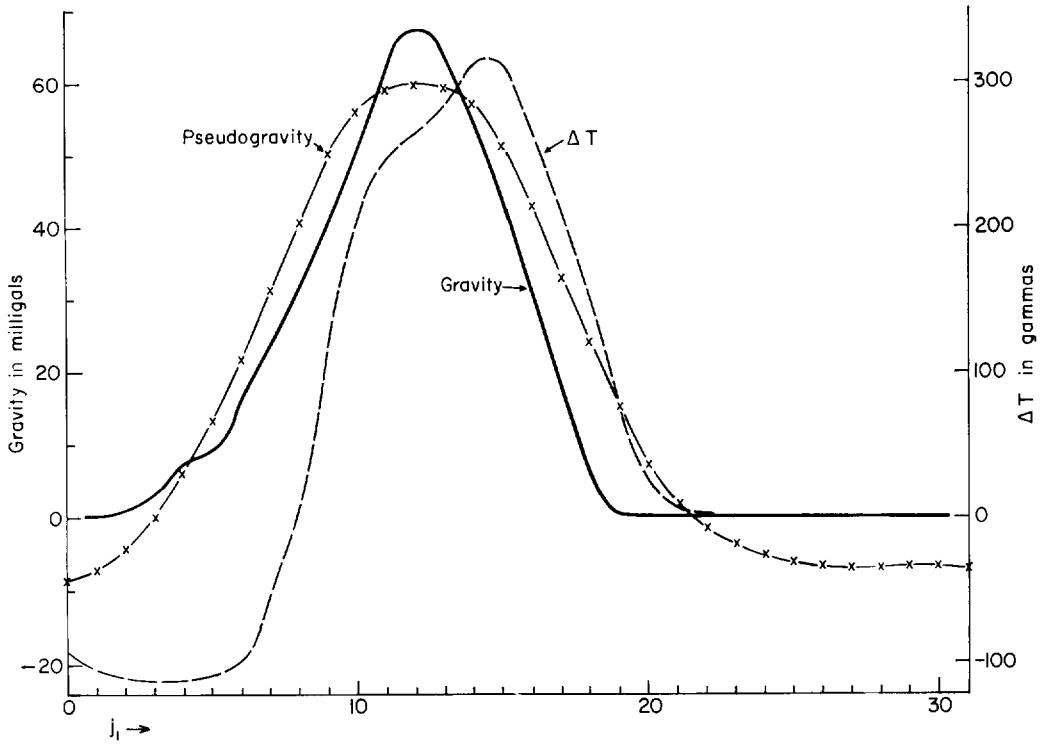

FIG. 10. East-west profile across Gilliss seamount along line indicated on Figure 9, showing magnetic, gravity, and pseudogravity profiles. Grid interval is 1.5625 km.

sp. and *Globotruncana* sp. from cores obtained during a cruise of the USNS *James M. Gilliss* in September, 1969 indicate that the minimum age of the seamount is Late Cretaceous—Maestrichtian (Ruth Todd, U.S. Geological Survey, written communication, 1970). All pole positions are in the general area of eastern Siberia, which is, broadly, the predicted position for a Cretaceous source in the northwestern Atlantic (Irving, 1964; Harrison et al, 1967).

Although we have sought here to develop a system of analysis which is independent of the shape of the causative body, we have, for comparison, determined total magnetization direction by the magnetic modeling method, using the system described by Talwani (1965) and his computer program which he has kindly supplied. In this method, one assumes that magnetization is reasonably uniform throughout the solid delimited by the bathymetry above a flat base at a depth, in this case, of 2700 fathoms. As we have suggested above, the top of the seamount may be relatively nonmagnetic. If so, this model may not be appropriate to the Gilliss case. From the analysis, we obtained

$$J = 8.49 \times 10^{-3} \text{ emu/cm}^3,$$

$$t_{0_1} = -0.2546,$$

$$t_{0_2} = -0.9330,$$

and

$$t_{0_3} = 0.2537.$$

Supplying the value $\Delta\rho = 1.5$ gm/cm^3, we obtain for these parameters the pseudogravity anomaly shown in Figure 13. In this case the position and trend of the pseudogravity do not correspond well with those of the actual gravity field (cf. Figures 9 and 13). The paleo-pole position for the magnetization direction determined by the modeling method and for an assigned Q of infinity is labeled "M" in Figure 12.

COMMENT

In-situ methods, such as those described here, offer a means of determining bulk physical properties of inaccessible bodies of rock. The analysis is accomplished in a matter of seconds of computer time, and the derived results can be of great use in the interpretation of geophysical data. However, the results depend on the fidelity of the model and, of course, on the validity of the bulk physical property concept itself. Thus, on the former grounds, the results may be inaccurate; and on the latter, they may be meaningless.

In the course of the analysis of the Gilliss seamount data, we found that probably neither the hypotheses of the method of magnetic modeling nor those of our system based on Poisson's relationship were completely satisfied. However, both methods yielded plausible results, which appear to be consistent with sample data, predicted pole position, and a certain amount of geological speculation. The spectral approach may have an advantage in that questionable higher order wavenumber terms (related to relatively shallow sources) can be eliminated from the solution. In contrast with the direct measurement of physical properties on samples, however, these methods do not provide a statistical measure of confidence.

ACKNOWLEDGMENTS

We wish to thank the officers and crew of the USNS *Shoup* for their assistance in carrying out the marine geophysical surveys. We are indebted to Frederick J. Vine (Department of Environmental Sciences, University of East Anglia, Norwich, England) for providing the magnetic property measurements, to Ruth Todd (U. S. Geological Survey, Washington, D. C.) for the paleontological data, and to Manik Talwani (Lamont-Doherty Geological Observatory of Columbia University) for supplying his three-dimensional magnetic modeling computer program. The man-

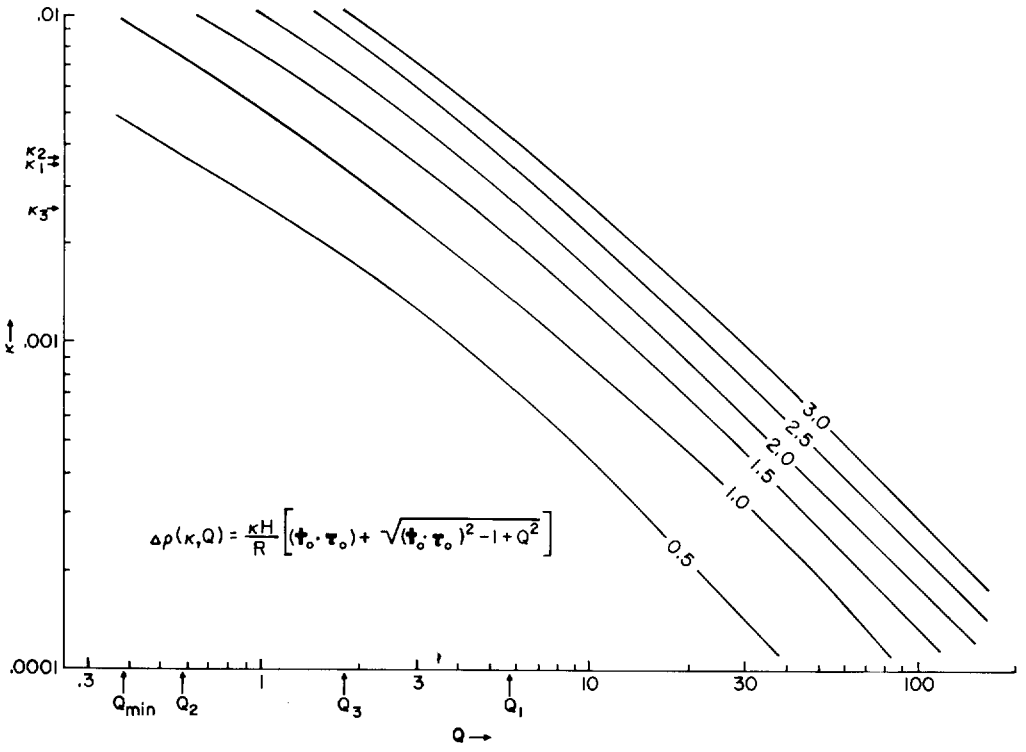

FIG. 11. Contour diagram of function $\Delta\rho(\kappa, Q)$ for Gilliss data. Both scales are logarithmic with decimal divisions. Contour interval is 0.5 gm/cm³.

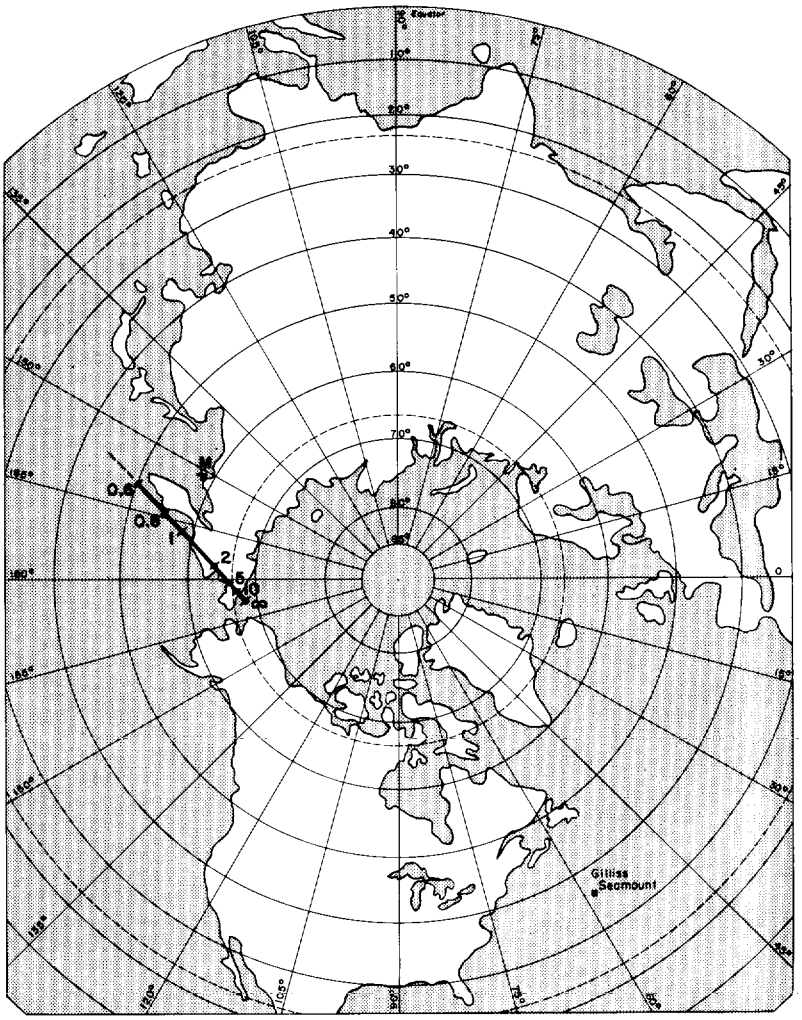

FIG. 12. Trace of paleomagnetic pole of Gilliss seamount as a function of Q. Pole positions corresponding to specific values of Q between 0.6 and infinity are labeled. Pole position as determined by method of magnetic modeling, for Q = infinity, is labeled "M".

uscript was typed by Mary F. Ohe, U. S. Geological Survey.

APPENDIX

In practice, the magnetic and gravity fields can only be represented analytically in terms of a grid of discrete values normally taken from contoured maps. The analysis leading to equation (9), however, is based on continuous functions defined on the entire plane. It is necessary, therefore, to complete the discrete data array in terms of an interpolated continuous function. Inasmuch as this operation is in a sense somewhat subjective, we choose a device here which will lead to a straightforward relationship between the integral and discrete Fourier transforms. A few more constraints on the data will be entailed.

In the case of the magnetic anomaly, we suppose that the actual field $\Delta T(x, y)$ is represented by the N_1 by N_2 sample array

$$\Delta T_{j_1 j_2} \equiv \Delta T(j_1 s, j_2 s);$$

$$\text{for } \begin{matrix} j_1 \\ j_2 \end{matrix} = 0, 1, \cdots \begin{matrix} N_1 - 1 \\ N_2 - 1 \end{matrix},$$

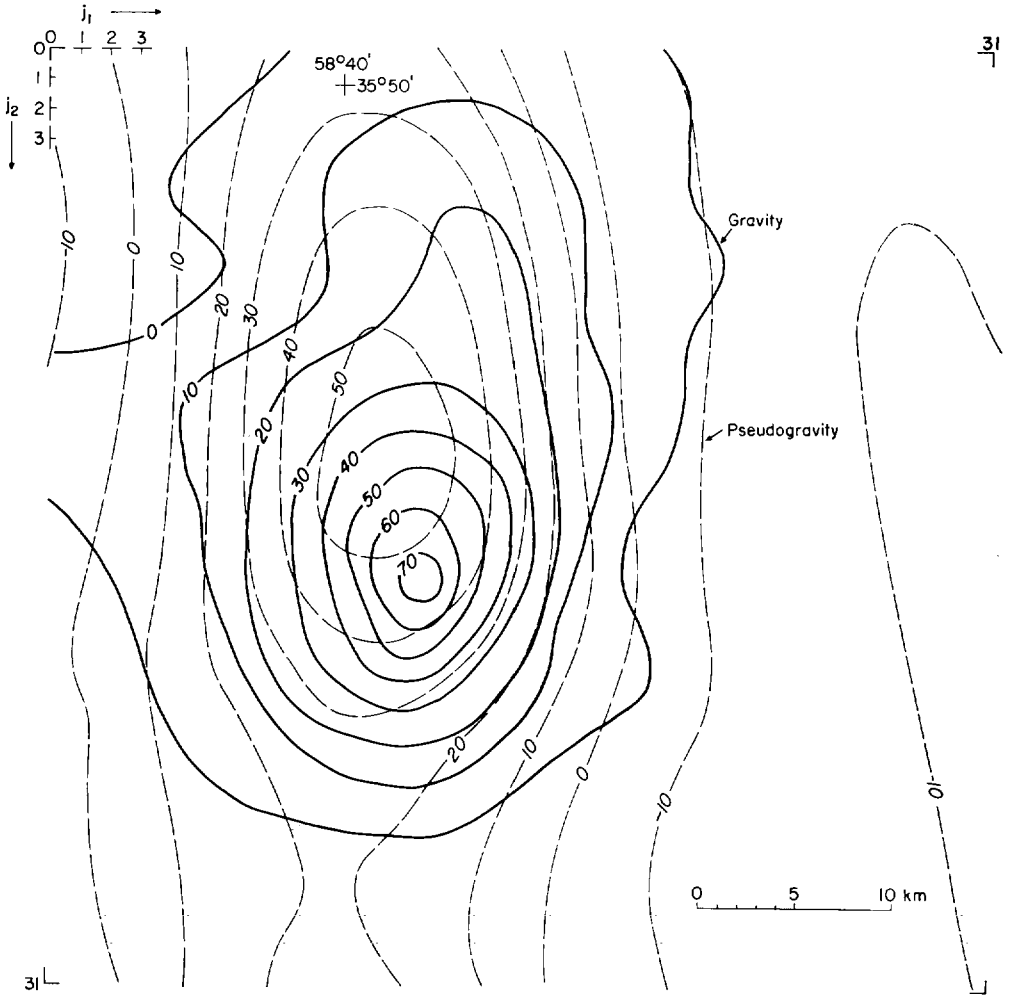

FIG. 13. Pseudogravity for Gilliss data based on magnetization direction determined by the method of magnetic modeling.

where s = grid interval. If we assume further that the field can be approximated by a band-limited function on the frequency interval $|\hat{x}| \leq 1/2s$, $|\hat{y}| \leq 1/2s$, we have, from the Shannon sampling theorem,

$$\Delta T(x, y) \simeq \sum_{j_1=-\infty}^{\infty} \sum_{j_2=-\infty}^{\infty} \Delta T_{j_1 j_2} \frac{\sin \pi\left(\frac{x}{s} - j_1\right)}{\pi\left(\frac{x}{s} - j_1\right)} \frac{\sin \pi\left(\frac{y}{s} - j_2\right)}{\pi\left(\frac{y}{s} - j_2\right)}.$$

Taking the Fourier transform of both sides yields

$$\Delta\widehat{T}(\hat{x}, \hat{y}) = \int\int_{-\infty}^{\infty} \Delta T(x, y)\, e^{2\pi i(x\hat{x}+y\hat{y})}\, dx dy$$

$$= s^2 \sum_{j_1=-\infty}^{\infty} \sum_{j_2=-\infty}^{\infty} \Delta T_{j_1 j_2}\, e^{-2\pi i(j_1\hat{x}+j_2\hat{y})s},$$

$$\text{for } |\hat{x}| < \frac{1}{2s}, \quad |\hat{y}| < \frac{1}{2s}.$$

If we assume finally that $\Delta T_{j_1 j_2}$ is approximately zero outside of the data grid $\substack{j_1=0,1\cdots N_1-1 \\ j_2=0,1\cdots N_2-1}$ and consider specific frequencies

$$0 \leq |\hat{x}_1| = \frac{k_1}{N_1} < \frac{1}{2};$$

$$0 \leq |\hat{y}_1| = \frac{k_2}{N_2} < \frac{1}{2},$$

we have, for unit grid interval $s=1$,

$$\Delta\hat{T}(\hat{x}_1, \hat{y}_1) \simeq \sum_{j_1=0}^{N_1-1} \sum_{j_2=0}^{N_1-1} \Delta T_{j_1 j_2} \cdot e^{-2\pi i\left(\frac{k_1 j_1}{N_1} + \frac{k_2 j_2}{N_2}\right)} = N_1 N_2 A^T_{k_1 k_2},$$

where A^T represents the discrete transform coefficient as given in equation (12). Thus, the analysis can be extended to the discrete domain, provided that the field can be approximated by a band-limited function. This, in turn, requires that the field is adequately sampled and that spurious discontinuities have not been introduced around the borders of the data grid.

The results discussed in the paper were obtained by means of a computer program written in Fortran for use on the Geological Survey's IBM 360-65 computer. The fast Fourier transform operation was effected by means of the IBM scientific subroutine DHARM, and the least squares solution of the linear equation matrix [equation (11)] was obtained by IBM scientific subroutine DLLSQ; these subroutines are described in IBM publication H20-0205-3: *System/360 Scientific Subroutine Package.*

Because both ΔT and Δg are real-valued functions, their discrete Fourier transforms can be obtained simultaneously by means of a telescoped system of analysis. We define on the points $j_1=0, 1, \cdots N_1-1$, and $j_2=0, 1, \cdots N_2-1$ the discrete complex function

$$F_{j_1 j_2} = \Delta T_{j_1 j_2} + i\Delta g_{j_1 j_2},$$

from which we obtain the discrete complex Fourier transform

$$A_{k_1 k_2} = \frac{1}{N_1 N_2} \sum_{j_1=0}^{N_1-1} \sum_{j_2=0}^{N_2-1} F_{j_1 j_2} \cdot e^{-2\pi i\left(\frac{k_1 j_1}{N_1} + \frac{k_2 j_2}{N_2}\right)}.$$

Making use of the spectral symmetry of the complex Fourier series, we then unscramble the $A_{k_1 k_2}$ coefficients in terms of the desired coefficients to get

$$\text{Re } A^T_{k_1 k_2} = \frac{1}{2}(\text{Re } A_{k_1 k_2} + \text{Re } A_{N_1-k_2,\, N_2-k_2}),$$

$$\text{Im } A^T_{k_1 k_2} = \frac{1}{2}(\text{Im } A_{k_1 k_2} - \text{Im } A_{N_1-k_1,\, N_2-k_2}),$$

$$\text{Re } A^g_{k_1 k_2} = \frac{1}{2}(\text{Im } A_{k_1 k_2} + \text{Im } A_{N_1-k_1,\, N_2-k_2}),$$

and

$$\text{Im } A^g_{k_1 k_2} = \frac{1}{2}(-\text{Re } A_{k_1 k_2} + \text{Re } A_{N_1-k_1,\, N_2-k_2}),$$

for $k_1 = 0, 1 \cdots N_1/2$ and $k_2 = 0, 1 \cdots N_2/2$.

Use of the telescoped analysis has the double advantage that both analyses are obtained by only one execution of the fast Fourier transform program, and that the minimum amount of computer core storage is required to contain the data arrays. About 3.6 sec of central processor time on the Geological Survey's IBM 360-65 computer were required to compile and execute the program for the examples discussed above.

REFERENCES

Baranov, V., 1957, A new method for interpretation of aeromagnetic maps: Pseudo-gravimetric anomalies: Geophysics, v. 22, p. 359–383.

Bhattacharyya, B. K., 1967, Some general properties of potential fields in space and frequency domain: A review: Geoexploration, v. 5, no. 3, p. 127–143.

Bott, M. H. P., Smith, R. A., and Stacey, R. A., 1966, Estimation of the direction of magnetization of a body causing a magnetic anomaly using a pseudo-gravity transformation: Geophysics, v. 31, p. 803–811.

Cooley, J. W., and Tukey, J. W., 1965, An algorithm for the machine calculation of complex Fourier series: Math. of Computation, v. 19, no. 90, p. 297–301.

Cordell, L., and Henderson, R. G., 1968, Iterative three-dimensional solution of gravity anomaly data using a digital computer: Geophysics, v. 33, p. 596–601.

Doell, R. R., and Cox, A., 1961, Paleomagnetism, *in* Advances in geophysics, v. 8, New York, Academic Press, p. 221–313.

Fabiano, E. B., and Peddie, N. W., 1969, Grid values of total-magnetic intensity IGRF-1965: U.S. ESSA Tech. Rep. C&GS 38, 1969, 55 p.

Garland, G. D., 1951, Combined analysis of gravity and magnetic anomalies: Geophysics, v. 16, p. 51–62.

Gentleman, W. M., and Sande, G., 1966, Fast Fourier transforms for fun and profit: American Federation of Information Processing Societies, Joint Computer Conference Proc., v. 29, Fall 1966, p. 563–578.

Grossling, B. F., 1967, The internal magnetization of seamounts and its computer calculation: USGS Prof. Paper 554-F, 26 p.

Harrison, C. G. A., Richards, M. L., and Vacquier, V., 1967, Paleomagnetism of submarine igneous rocks, *in* International dictionary of geophysics: S. K. Runcorn, ed., New York, Pergamon Press.

Henderson, R. G., and Allingham, J. W., 1964, The magnetization of an inhomogeneous laccolith calculated on a digital computer, *in* Computers in the mineral industries, part 2: Stanford Univ. Pubs. Geol. Sci., v. 9, p. 479–481.

Irving, E., 1964, Paleomagnetism and its application to geological and geophysical problems: New York, John Wiley and Sons, 399 p.

Kanasewich, E. R., and Agarwal, R. G., 1970, Analysis of combined gravity and magnetic fields in wave-number domain: J. Geophys. Res., v. 75, p. 5702–5712.

LaFehr, T. R., 1965, The estimation of the total amount of anomalous mass by Gauss's theorem: J. Geophys. Res., v. 70, p. 1911–1919.

Talwani, M., 1965, Computation with the help of a digital computer of magnetic anomalies caused by bodies of arbitrary shape: Geophysics, v. 30, p. 797–817.

Talwani, M., and LePichon, X., 1969, Gravity field over the Atlantic Ocean: Am. Geophys. Union, Geophys. Mon. 13, p. 341–351.

Taylor, P. T., and Hekinian, R., 1971, Geology of a newly discovered seamount in the New England seamount chain: Earth and Planetary Sci. Letters, v. 11, no. 2, p. 73–82.

Vacquier, V., 1962, A machine method for computing the magnitude and the direction of magnetization of a uniformly magnetized body from its shape and a magnetic survey, *in* Benedum earth magnetism symposium, Pittsburgh, Pa., 1962, Proc. Pittsburgh, Univ. Pittsburgh Press, p. 123–137.